

Dielectric and impedance study of lead-free ceramic: (Na_{0.5}Bi_{0.5})ZrO₃

Lily · K. Kumari · K. Prasad · K. L. Yadav

Received: 8 June 2006 / Accepted: 21 August 2006 / Published online: 21 April 2007
© Springer Science+Business Media, LLC 2007

Abstract Polycrystalline sample of (Na_{0.5}Bi_{0.5})ZrO₃ was prepared using a high-temperature solid-state reaction technique. XRD analysis indicated the formation of a single-phase orthorhombic structure. Dielectric study revealed the diffuse phase transition at 425 °C. AC impedance plots were used as tools to analyse the electrical behaviour of the sample as a function of frequency at different temperatures. The ac impedance studies revealed the presence of grain boundary effect at and above 350 °C. Complex impedance analysis indicated non-Debye type dielectric relaxation and negative temperature coefficient of resistance (NTCR) character of (Na_{0.5}Bi_{0.5})ZrO₃. AC conductivity data were used to evaluate the density of states at Fermi level and activation energy of the compound. DC electrical and thermal conductivities of grain and grain boundary have been assessed.

Introduction

Sodium bismuth titanate, (Na_{0.5}Bi_{0.5})TiO₃ (NBT) showing ferroelectricity at room temperature, having high Curie temperature at 320 °C, is considered to be a promising candidate for various electronic devices such as multilayer capacitors (MLCCs), piezoelectric transducers, pyroelec-

tric detectors/sensors, electrostrictive actuators, precision micropositioners, MEMs, etc. [1–3]. NBT belongs to perovskite family (ABO₃-type) with rhombohedral symmetry at ambient temperature. NBT received considerable attention for the past several years due to its superior ferroelectric/piezoelectric properties as compared to the most widely used piezoelectric ceramics like PbTiO₃–PbZrO₃. Besides, lead and its compounds are listed as toxic and hazardous in the form of direct pollution originating from the waste produced during manufacturing and machining of the components. Besides, products containing Pb-based gadgets are not recyclable. Taking into consideration the environmental, health and social aspects, manufacturers have been constrained to reduce and ultimately eliminate the Pb-content of the materials. Hence, the search for alternative materials for MLCCs, piezoelectric/pyroelectric applications has now become a focal theme of the present day research. Further, titanate-based materials are of interest as they are suitable for room temperature applications mainly due to their dielectric properties. Their low temperature behaviour is often controlled by grain boundaries. Therefore, the knowledge of behaviour of grain boundary is important. Complex impedance spectroscopic technique is considered to be a promising non-destructive testing method for analysing the electrical processes occurring in a compound on the application of ac signal as input perturbation. The output response of polycrystalline compound plotted in a complex plane, represents grain, grain boundary and electrode properties with different time constants, leading to successive semicircles.

During the past few years, several investigations have been made to study the electrical properties of the solid solutions of (Na_{0.5}Bi_{0.5})TiO₃ with different perovskites like: BaTiO₃ [4–8], SrTiO₃ [6, 9–11], PbTiO₃ [12, 13], CaTiO₃ [14], (K_{0.5}Bi_{0.5})TiO₃ [13, 15, 16], (K_{0.5}Bi_{0.5})TiO₃–

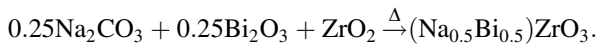
Lily · K. Kumari · K. Prasad (✉)
Materials Research Laboratory, University Department of
Physics, T. M. Bhagalpur University, Bhagalpur 812 007, India
e-mails: k_prasad65@yahoo.co.in; k.prasad65@gmail.com

K. L. Yadav
Department of Physics, Indian Institute of Technology, Roorkee
247 667, India

BaTiO₃ [17, 18], etc. for their possible applications in electronic devices. All these attempts have been made to modify *A*-site i.e. divalent pseudo-cation (Na, Bi)²⁺. Further, it has been observed that modification at *B*-site plays an important role in tailoring various properties of perovskite [19–22]. An extensive literature survey suggested that no attempt, to our knowledge, has so far been made to replace Ti⁴⁺ by Zr⁴⁺ ion. Accordingly, the present work reports the structural, dielectric, impedance and conductivity studies on (Na_{0.5}Bi_{0.5})ZrO₃ (abbreviated hereafter as NBZ) ceramic. Further, an attempt have been made to study the role of grain and grain boundaries on electrical properties of NBZ and their dependence on temperature and frequency, using complex impedance spectroscopy technique.

Experimental

(Na_{0.5}Bi_{0.5})ZrO₃ was obtained from AR grade (99.9%+ pure) chemicals (Na₂CO₃, Bi₂O₃ and ZrO₂) by solid-state synthesis using the following chemical reaction at 1,070 °C for 4 h:



Circular disc shaped pellet having geometrical dimensions: thickness = 1.6 mm and diameter = 11.34 mm was made by applying uniaxial stress of 6 MPa. The pellet was subsequently heated up to 1,100 °C under oxygen for 3 h. Completion of the reaction and the formation of the desired compound were checked by X-ray diffraction technique. The XRD spectra were taken on calcined powders of NBZ with an X-ray diffractometer (Rikagu Miniflex, Japan) at room temperature, using CuK_α radiation ($\lambda = 0.15418$ nm), over a wide range of Bragg angles ($20^\circ \leq 2\theta \leq 80^\circ$) with a scanning speed of 2° min^{-1} . The electrical measurements were carried out on a symmetrical cell of type Ag|NBZ|Ag, where Ag is a conductive paint coated on either side of the pellet. Electrical impedance (*Z*), phase angle (θ), loss tangent ($\tan\delta$) and capacitance (*C*) were measured as a function of frequency (0.1 kHz–2 MHz) at different temperatures (40–500 °C) using a computer-controlled LCR Hi-Tester (HIOKI 3532-50), Japan.

Results and discussion

Structural study

A standard computer program (POWD) was utilized for the XRD-profile (Fig. 1) analysis. Good agreement between

the observed and calculated inter-planer spacing (*d*-values) and no trace of any extra peaks due to constituent oxides, were found, thereby suggesting the formation of a single-phase compound having an orthorhombic structure. The lattice parameters were found to be: $a = 4.379(7)$ Å, $b = 7.489(5)$ Å and $c = 7.078(3)$ Å with an estimated error of $\pm 10^{-3}$ Å. The criterion adopted for evaluating the correctness, reliability of the indexing and the structure of NBZ was the evaluation of sum of differences in observed and calculated *d*-values [i.e. $\Sigma\Delta d = \Sigma(d_{\text{obs}} - d_{\text{calc}})$] which was found to be a minimum in the present case. The unit cell volume ($a \times b \times c$) was estimated to be 232.18 Å³.

Dielectric studies

The value of dielectric constant of NBZ was obtained using the relation: $\epsilon = Cl/\epsilon_0 A$, where *l* is the thickness and *A* is the surface area of the specimen. Figure 2a, b, respectively, show the frequency dependence of ϵ' and ϵ'' at several temperatures. It is observed that both ϵ' as well as ϵ'' follow inverse dependence on frequency, normally followed by almost all dielectric/ferroelectric materials. Further, both the pattern presents the dispersion in the lower frequency range. The Debye formula giving the complex permittivity, related to free dipole oscillating in an alternating field, is as follows:

$$\epsilon^* = \epsilon' - i\epsilon'' = \epsilon_\infty + \frac{\epsilon_s - \epsilon_\infty}{1 + i\omega\tau}. \quad (1)$$

The real part of ϵ is given by

$$\epsilon' = \epsilon_\infty + \frac{\epsilon_s - \epsilon_\infty}{1 + \omega^2\tau^2}, \quad (2)$$

where ϵ_s and ϵ_∞ are the low and high frequency values of ϵ' , $\omega = 2\pi f$, *f* being the frequency of measurement and τ the relaxation time. A relatively high dielectric constant at low frequencies is a characteristic of a dielectric material. At very low frequencies ($\omega \ll 1/\tau$), dipoles follow the field and we have $\epsilon' \approx \epsilon_s$ (value of dielectric constant at quasi static fields). As the frequency increases (with $\omega < 1/\tau$), dipoles begin to lag behind the field and ϵ' slightly decreases. When frequency reaches the characteristic frequency ($\omega = 1/\tau$), the dielectric constant drops (relaxation process). At very high frequencies ($\omega \gg 1/\tau$), dipoles can no longer follow the field and $\epsilon' \approx \epsilon_\infty$. Qualitatively, the same behaviour is observed in the material studied in the present work as shown in Fig. 2a.

The temperature dependence of real and imaginary part of dielectric constant at different frequencies is shown in Fig. 3. All the plots show a broad ferro-paraelectric phase transition (i.e. diffuse phase transition, DPT) at 425 °C. It is found that both real and imaginary parts of dielectric

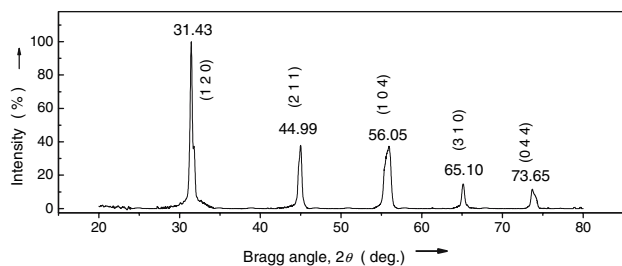


Fig. 1 Indexed X-ray diffraction pattern of $(\text{Na}_{0.5}\text{Bi}_{0.5})\text{ZrO}_3$ at room temperature

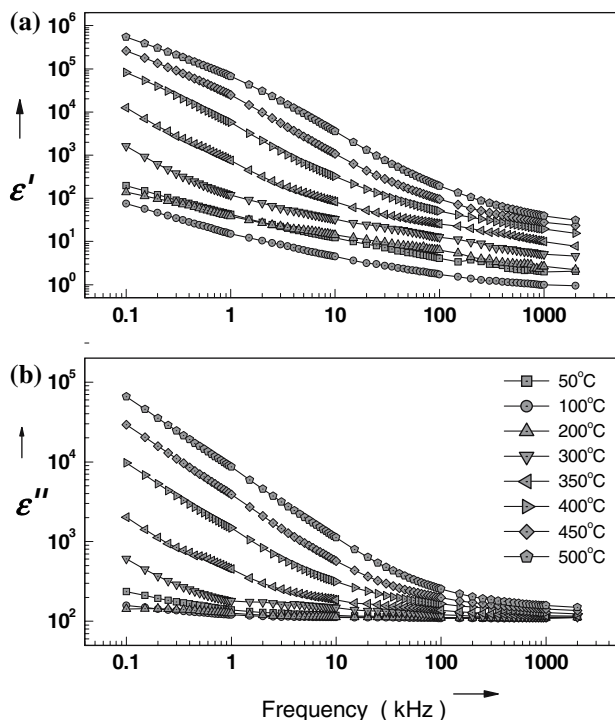


Fig. 2 Frequency dependence of (a) real and (b) imaginary part dielectric constant of $(\text{Na}_{0.5}\text{Bi}_{0.5})\text{ZrO}_3$ at different temperature

constant at room temperature as well as at T_c decrease with increasing frequency. Also, $\epsilon'-T$ and $\epsilon''-T$ curves flatten i.e. diffusivity increases with increasing frequency. The dielectric peak broadening is a common occurrence in solid solutions with disordered structures. The multiple ion occupation at different sites causes deviation from normal Curie–Weiss behaviour, where T_c is not sharp, but physical properties change rather gradually over a temperature range, and is known as DPT. The DPT can be explained by modified Curie–Weiss law:

$$1/\epsilon' - 1/\epsilon'_{\max} = A(T - T_c)^\gamma, \quad (3)$$

where A is a constant and γ is the diffusivity exponent which can vary from 1, for normal to 1–2 for DPT. A linear

least squares fitting of dielectric data to Eq. 3 have given the value of $\gamma > 1.45$, clearly indicating the presence of DPT in the system. This may be due to presence of more than one cation in the sub-lattice that should produce some kind of heterogeneities.

Impedance studies

Figure 4 shows the variation of the real (Z') and imaginary (Z'') part of impedance with frequency at various temperatures. It is observed that the magnitude of Z' decreases with the increase of both frequency as well as temperature indicates an increase in ac conductivity with the rise in temperature and frequency. The Z' values for all temperatures almost coalesce at and above 100 kHz. This may be due to the release of space charges produced as a result of reduction in the barrier properties of material with the rise in temperature and may be a responsible factor for the enhancement of ac conductivity of material with temperature at higher frequencies. Further, at low frequencies the Z' values decrease with rise in temperature, indicating the negative temperature coefficient of resistance (NTCR) behaviour like that of semiconductors. The variation of the imaginary part of impedance with frequency at different temperatures, shows that the Z'' values reach a maxima peak (Z''_{\max}) for the temperatures $\geq 300^\circ\text{C}$ and the value of Z''_{\max} shifts to higher frequencies with increasing temperature. A typical peak-broadening, which is slightly asymmetrical in nature, can be observed with the rise in temperature. The broadening of peaks in frequency explicit plots of Z'' suggests that there is a spread of relaxation times i.e., the existence of a temperature dependent electrical relaxation phenomenon in the material is exhibited [23].

Figure 5 shows a set of impedance data taken over a wide frequency range at several temperatures as a Nyquist diagram (complex impedance spectrum). It is observed that with the increase in temperature the slope of the lines decreases and they bend towards real (Z') axis and at 300°C , a semicircle could be traced, indicating the increase in conductivity of the sample. At and above 350°C , two semicircles could be obtained with different values of resistance for grain (R_b) and grain boundary (R_{gb}). Hence, grain and grain boundary effects could be separated at these temperatures. It can also be observed that the peak maxima of the plots decrease and the frequency for the maximum shifts to higher values with the increase in temperature. The polydispersive (non-Debye type) nature of dielectric relaxation could be judged through complex impedance plots. For pure monodispersive Debye relaxation, one expects semicircular plots with the centre located on the Z' -axis, whereas for polydispersive relaxation these argand plane plots are close to semicircular arcs with

Fig. 3 Temperature dependence of real and imaginary part of dielectric constant of $(\text{Na}_{0.5}\text{Bi}_{0.5})\text{ZrO}_3$ at different frequency

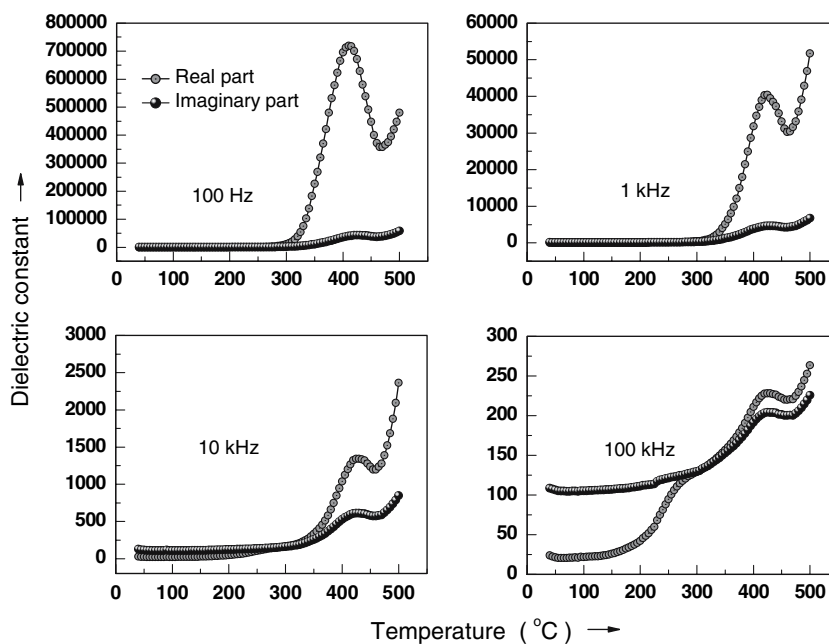
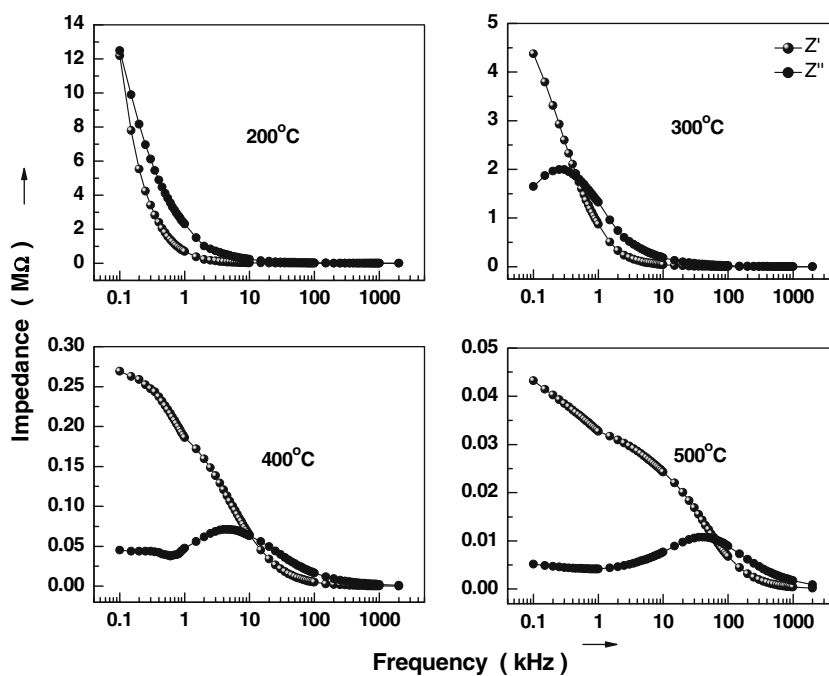


Fig. 4 Frequency dependence of real and imaginary part of impedance of $(\text{Na}_{0.5}\text{Bi}_{0.5})\text{ZrO}_3$ at different temperature



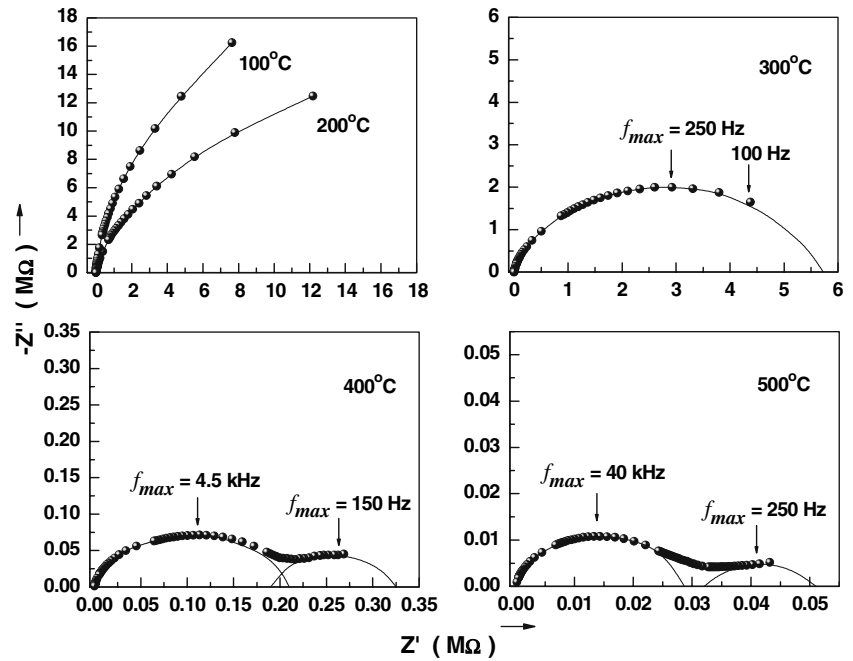
end-points on the real axis and the centre lying below this axis. The complex impedance in such situations can be described as:

$$Z^*(\omega) = Z' + iZ'' = R/[1 + (i\omega/\omega_0)^{1-\alpha}], \tag{4}$$

where α represents the magnitude of the departure of the electrical response from an ideal condition and this can be determined from the location of the centre of the semicircles. When α goes to zero (i.e. $(1 - \alpha) \rightarrow 1$), Eq. 4 gives rise to classical Debye’s formalism. It can be

noticed that the complex impedance plots are not represented by full semicircle, rather the semicircular arc is depressed and the centre of the arc lies below the real (Z') axis ($\alpha > 0$) suggesting the relaxation to be of polydispersive non-Debye type in NBZ. This may be due to the presence of distributed elements in the material-electrode system [24]. Also, the value of α increases with the rise in temperature. The correlation among the Debye relaxators may start developing via formation of nanopolar clusters of Na–ZrO₃ and Bi–ZrO₃ [25]. Since the relaxation

Fig. 5 Cole–Cole plot of $(\text{Na}_{0.5}\text{Bi}_{0.5})\text{ZrO}_3$ at different temperature



times of the relaxators within polar clusters are distributed over a wide spectrum at higher temperatures, their response to external field are in a different time domain. This results in the deviation from Cole–Cole plots. It is clear from Fig. 5 that with the increase of measuring temperature Cole–Cole plots become stretched and/or splitted into two discrete semicircles, inferring the possible average profile of various Cole–Cole semicircles. The splitted as well as stretched semicircles may be due to secondary elements like interfacial capacitance or defects. The values of R_b and R_{gb} could directly be obtained from the intercept on the Z' -axis whose variation with temperature are shown in Fig. 6. It can be noticed that the value of R_b and R_{gb} decrease with

the rise of temperature, which clearly indicates the NTCR character of NBZ and supports Fig. 4. The capacitances (C_b and C_{gb}) due to these effects can be calculated using the relation:

$$\omega_{\max}RC = 1, \quad (5)$$

where $\omega_{\max} (= 2\pi f_{\max})$ is the angular frequency at the maximum of the semicircle. Figure 6 shows the temperature variation of C_b and C_{gb} obtained from Cole–Cole plots at different temperatures. The relaxation times ($\tau = 1/\omega_{\max}$) were estimated from the maximum of the semicircles due to grain as well as grain boundary effects in the complex impedance plots (Fig. 5). The temperature variation of relaxation times due to bulk and grain boundary effects (Fig. 7) follows the Arrhenius relationship:

$$\tau = \tau_0 \exp(-E_\tau/k_B T), \quad (6)$$

where τ_0 is the pre-exponential factor. The activation energy, E_τ calculated from linear least squares fit to $\log \tau - 1/T$ data is 0.42 and 0.11 eV, respectively, for bulk and grain boundary.

Figure 8 shows the plot of scaled Z'' vs. $\log f$ [i.e., Z''/Z''_{\max} and $\log(f/f_{\max})$], where f_{\max} corresponds to the peak frequency of the Z'' vs. $\log f$ plots. It can be seen that the Z'' -data coalesced into a master curve. The value of full width at half maximum (FWHM) is found to be >1.14 decades. These observations indicate that the distribution function for relaxation times is nearly temperature independent with non-exponential conductivity relaxation,

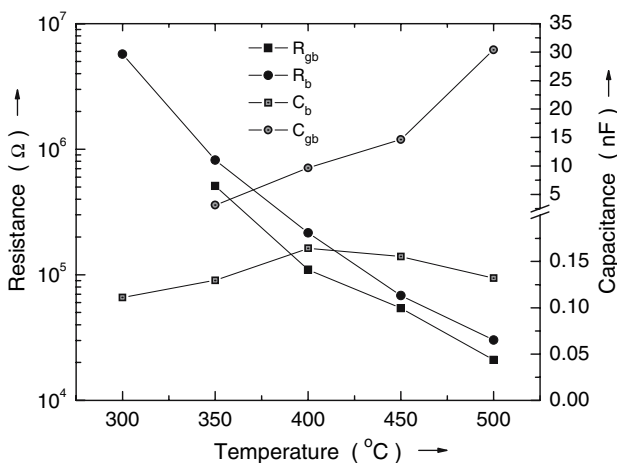


Fig. 6 Variation of R_g , R_{gb} , C_g and C_{gb} with temperature of $(\text{Na}_{0.5}\text{Bi}_{0.5})\text{ZrO}_3$

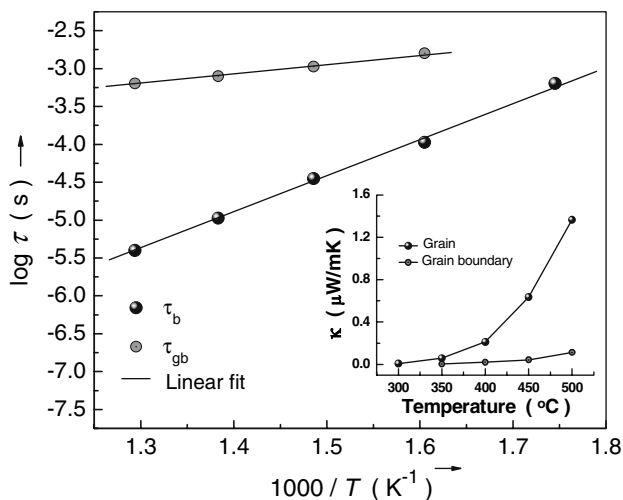


Fig. 7 Temperature dependence of bulk and grain boundary relaxation times for $(\text{Na}_{0.5}\text{Bi}_{0.5})\text{ZrO}_3$. Inset: Variation of thermal conductivity of grain and grain boundary with temperature

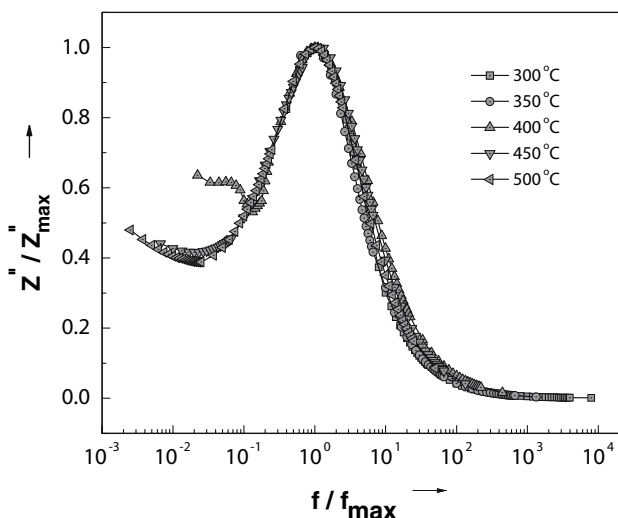


Fig. 8 Scaling behaviour of Z'' for $(\text{Na}_{0.5}\text{Bi}_{0.5})\text{ZrO}_3$

which suggests the possibility of ion migration that takes place via hopping accompanied by a consequential time-dependent mobility of other charge carriers of the same type in the vicinity [26].

Figure 9 shows the variation of scaled parameters ($\tan \delta / \tan \delta_{\max}$, Z''/Z''_{\max} and M''/M''_{\max}) with frequency at 500 °C. It can be seen that the peaks are not occurring at the same frequency ($f_{\tan \delta} < f_{Z''} < f_{M''}$). The magnitude of mismatch between the peaks of these parameters represents a change in the apparent polarization. The overlapping of peaks is an evidence of long-range conductivity whereas the difference is an indicative of short-range conductivity (via hopping type of mechanism) [27].

Conductivity studies

The ac electrical conductivity was obtained in accordance with the following relation:

$$\sigma_{ac} = l/SZ', \tag{7}$$

where l is the thickness and S is the surface area of the specimen. Figure 10 shows the electrical conductivity σ_{ac} of NBZ as a function of frequency at different temperature. The conductivity depends on frequency according to the ‘‘universal dynamic response’’ given by the phenomenological law:

$$\sigma_{ac} = \sigma(0) + K \cdot \omega^s, \tag{8}$$

where K is a thermally activated quantity and s is the frequency exponent and can take a value less than 1. This indicates that the conduction process is a thermally activated process. It is observed that variation of σ_{ac} with frequency shows flattening with increment in temperature (≥ 300 °C). The switch over from the frequency-independent $\sigma(0)$ to the dependent σ_{ac} regions shows the onset of the conductivity relaxation phenomenon and the translation from long range hopping to the short-range ion motion [28]. The dispersion in conductivity at low frequencies may be due to the electrode polarization. Further, it is observed that the electrical conductivity increases with the increase in temperature.

Figure 11 shows the variation of ac as well as dc ($\sigma_{dc} = l/SR_b$) conductivities ($\ln \sigma$) vs. $10^3/T$. The activation energy for conduction was obtained using the Arrhenius relationship:

$$\sigma = \sigma_0 \exp(-E_a/k_B T). \tag{9}$$

The variation of E_a with temperature obtained using least squares fitting of the conductivity data to Eq. 9 is shown in the inset Fig. 11. It is observed that the value of E_a decreases with the increase in frequency and it is less than $E_a(\text{dc})$. The low value of activation energy obtained could be attributed to the influence of electronic contribution to the conductivity. The increase in conductivity with temperature may be considered on the basis that within the bulk, the oxygen vacancies due to the loss of oxygen are usually created during sintering and the charge compensation follows the reaction (Kröger and Vink [29]): $O_o \rightarrow 1/2 O_2 \uparrow + V_o^{\bullet\bullet} + 2e^-$, which may leave behind free electrons, making them n-type [30]. The low value of $E_a(\text{ac})$ may be due to the carrier transport through hopping between localized states in a disordered manner. The temperature variations of thermal conductivity of grain and grain boundary for NBZ are shown in the inset of Fig. 7.

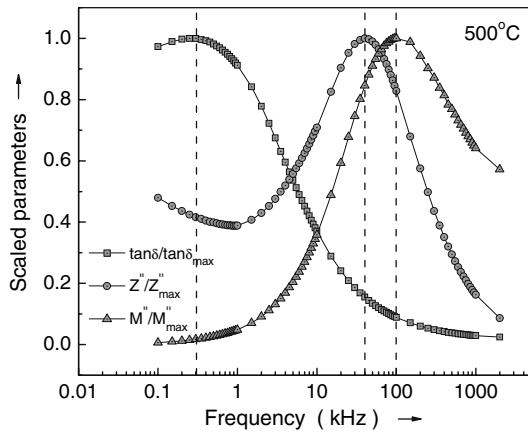


Fig. 9 Variation of normalized $\tan\delta$, Z'' and M'' with frequency of $(\text{Na}_{0.5}\text{Bi}_{0.5})\text{ZrO}_3$ at 500°C

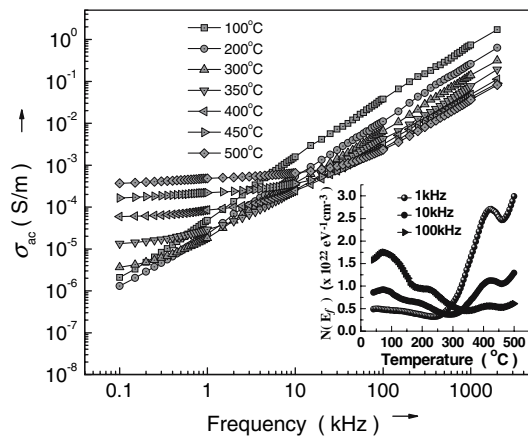


Fig. 10 Variation of ac conductivity with frequency at different temperature for $(\text{Na}_{0.5}\text{Bi}_{0.5})\text{ZrO}_3$. Inset: Variation of $N(E_f)$ of $(\text{Na}_{0.5}\text{Bi}_{0.5})\text{ZrO}_3$ with temperature at 1, 10 and 100 kHz

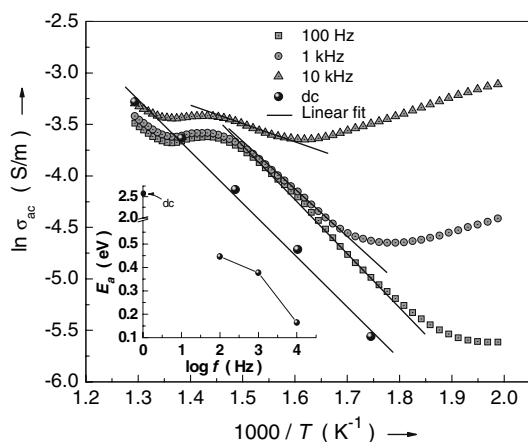


Fig. 11 Variation of ac conductivity (ac and dc) with inverse of temperature for $(\text{Na}_{0.5}\text{Bi}_{0.5})\text{ZrO}_3$. Inset: Frequency dependence of activation energy

NBZ represents a semiconductor behaviour resulting in an increased electronic conduction of the total thermal conductivity. This electronic thermal conductivity accounts for the total thermal conductivity [31] and is given by:

$$\kappa = L\sigma T[1 + (3/4\pi^2)\{(E_a/k_B T) + 4\}^2], \quad (10)$$

where L is the Lorentz number. It is observed that the thermal conductivity of grain as well as grain boundary increases with increasing temperature and it exhibits a reasonably low thermal conductivity.

The ac conductivity data have been used to evaluate the density of states at Fermi level $N(E_f)$ using the relation [32]:

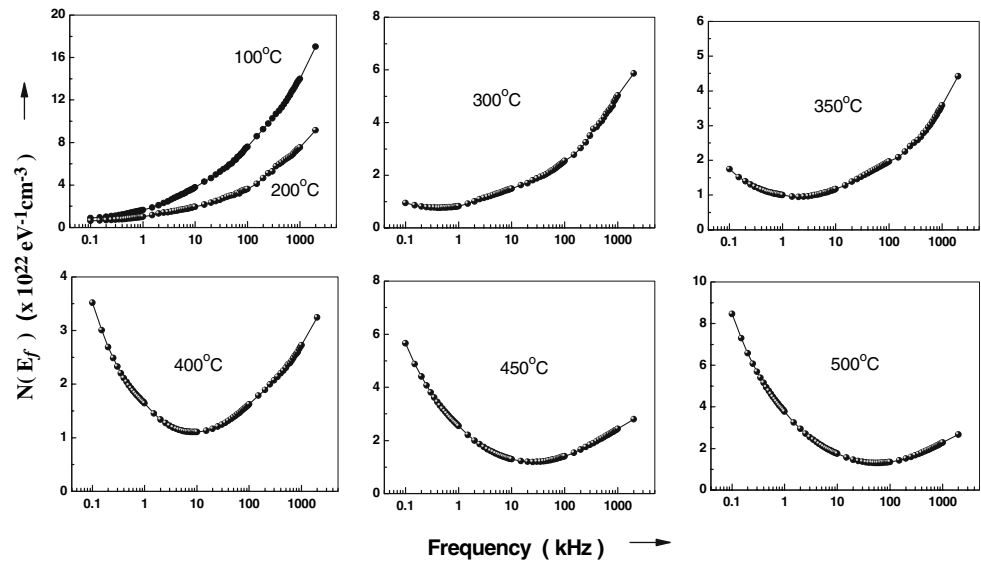
$$\sigma_{ac}(\omega) = \frac{\pi}{3} e^2 \omega k_B T \{N(E_f)\}^2 \alpha^{-5} \left\{ \ln \left(\frac{f_0}{\omega} \right) \right\}^4, \quad (11)$$

where e is the electronic charge, f_0 the photon frequency and α is the localized wave function, assuming $f_0 = 10^{13}$ Hz, $\alpha = 10^{10} \text{ m}^{-1}$ at various operating frequencies and temperatures. Figure 12 shows the Frequency dependence of $N(E_f)$ at different temperature. It can be seen that the value of $N(E_f)$ increases with the increase in operating frequency up to 200°C . At and above 300°C , each of the plots shows a minimum and a perfect minimum can be seen at 400°C and after this temperature the minimum starts disappearing. Further, it can be noticed the minima shift towards higher frequency side with the rise in temperature. Inset Fig. 10 illustrates the variation of $N(E_f)$ with temperature at 1 kHz. It is observed that the value of $N(E_f)$ decreases up to 300°C and thereafter, it increases with the rise in temperature. Also, the $N(E_f)$ minima shift to higher temperature side with the increase in frequency. The reasonably high values of $N(E_f)$ suggest that the hopping between the pairs of sites dominates the mechanism of charge transport in NBZ.

Conclusion

Polycrystalline $(\text{Na}_{0.5}\text{Bi}_{0.5})\text{ZrO}_3$, prepared through a high-temperature solid-state reaction technique, was found to have a single-phase perovskite-type orthorhombic structure. Dielectric study revealed the phase transition at 425°C with diffusive character. Impedance analyses indicated the presence of grain and grain boundary effect in NBZ. The value of full width at half maximum (FWHM) is found to be >1.14 decades, indicating the distribution of relaxation times to be nearly temperature independent with non-exponential conductivity relaxation. Sample showed dielectric relaxation, which is found to be of non-Debye type and the relaxation frequency shifted to higher side with the increase of temperature. The Nyquist plot and

Fig. 12 Variation of $N(E_f)$ of $(\text{Na}_{0.5}\text{Bi}_{0.5})\text{ZrO}_3$ with frequency at different temperature



conductivity studies showed the NTCR character of NBZ. The ac conductivity is found to obey the universal power law. The barrier hopping model is found to successfully explain the mechanism of charge transport in NBZ. Further, the frequency dependent ac conductivity at different temperatures indicated that the conduction process is thermally activated process.

References

1. Bührer CF (1962) *J Chem Phys* 36:798
2. Suchanicz J, Roleder K, Kania A, Handerek J (1988) *Ferroelectrics* 77:107
3. Roleder K, Suchanicz J, Kania A (1989) *Ferroelectrics* 89:1
4. Hosono Y, Harada K, Yamashita Y (2001) *Jpn J Appl Phys* 40:5722
5. Suchanicz J, Kusz J, Böhöm H, Duda H, Mercurio JP, Konieczny K (2003) *J Euro Ceram Soc* 23:1559
6. Gomah-Petry JR, Saïd S, Marchet P, Mercurio JP (2004) *J Euro Ceram Soc* 24:1165
7. Xu Q, Chen S, Chen W, Wu S, Zhou J, Sun H, Li Y (2005) *Mater Chem Phys* 90:111
8. Ranjan R, Dwiwedi A (2005) *Solid State Commun* 135:394
9. Gomah-Petry JR, Salak AN, Marchet P, Ferreira VM, Mercurio JP (2004) *Phys Stat Sol (b)* 241:1949
10. Park SE, Hong KS (1997) *J Mater Res* 129:279
11. Lee JK, Hong KS, Kim CK, Park SE (2002) *J Appl Phys* 91:4538
12. Saïd S, Marchet P, Merle-Méjean T, Mercurio JP (2004) *Mater Lett* 58:1405
13. Saïd S, Mercurio JP (2001) *J Euro Ceram Soc* 21:1333
14. Saradhi BVB, Srinivas K, Bhimasankaram T (2002) *Int J Mod Phys B* 16:1
15. Li Y, Chen W, Zhou J, Xu Q, Sun H, Liao M (2005) *Ceram Int* 31:139
16. Yoo J, Oh D, Jeong Y, Hong J, Jung M (2004) *Mater Lett* 58:3831
17. Li Y, Chen W, Xu Q, Zhou J, Gu X, Fang S (2005) *Mater Chem Phys* 94:328
18. Li YM, Chen W, Xu Q, Zhou J, Gu X (2005) *Mater Lett* 59:1361
19. Li YM, Chen W, Zhou J, Xu Q, Gu XY, Liao RH (2005) *Physica B* 365:76
20. Li Y, Chen W, Zhou J, Xu Q, Sun H, Xu R (2004) *Mater Sci Eng B* 112:5
21. Wada T, Toyoiike K, Imanaka Y, Matsuo Y (2001) *Jpn J Appl Phys* 40:5703
22. Ishii H, Nagata H, Takenaka T (2001) *Jpn J Appl Phys* 40:5660
23. Suman CK, Prasad K, Choudhary RNP (2005) *Adv Appl Ceram* 104:294
24. Macdonald JR (ed) (1987) *Impedance spectroscopy: emphasizing solid materials and systems*. John Wiley and Sons, New York
25. Bonneau P, Garnier O, Calvarin G, Husson E, Gavarrri JR, Hewat AW, Morrel A (1991) *J Solid State Chem* 91:350
26. Prasad K, Kumar A, Choudhary SN, Choudhary RNP (2005) *Solid State Ionics* 176:1641
27. Nobre MAL, Lanfredi S (2003) *J Phys Chem Solids* 64:2457
28. Grigas J (1996) *Microwave dielectric spectroscopy of ferroelectrics and related materials*. Gordon and Breach Pub. Inc., Amsterdam
29. Kröger FA, Vink HJ (1956) *Solid State Phys* 3:307
30. Prasad K, Suman CK, Choudhary RNP (2005) *Ferroelectrics* 324:89
31. E-Abd El-Wahabb (2000) *Vacuum* 57:339
32. Austin IG, Mott NF (1969) *Adv Phys* 18:41